JACS
JOURNAL OF THE AMERICAN CHEMICAL SOCIETY
Article
pubs.acs.org/JACS

Porphyrins Fused with Strongly Electron-Donating 1,3-Dithiol-2-ylidene Moieties: Redox Control by Metal Cation Complexation and Anion Binding

Nathan L. Bill,[†] Masatoshi Ishida,[‡] Steffen Bähring,[§] Jong Min Lim,[‡] Sangsu Lee,[‡] Christina M. Davis,[†] Vincent M. Lynch,[†] Kent A. Nielsen,[§] Jan O. Jeppesen,[§] Kei Ohkubo,[∥] Shunichi Fukuzumi,*[,∥,⊥] Dongho Kim,*[,‡] and Jonathan L. Sessler*[,†,‡]

[†]Department of Chemistry and Biochemistry, University Station-A5300, The University of Texas at Austin, Austin, Texas 78712, United States

[‡]Department of Chemistry, Yonsei University, Seoul 120-750, Korea

[§]Department of Physics, Chemistry and Pharmacy, University of Southern Denmark, 5230 Odense M, Denmark

[∥]Department of Material and Life Science, Graduate School of Engineering, Osaka University, ALCA, Japan Science and Technology Agency, Suita, Osaka 565-0871, Japan

[⊥]Department of Bioinspired Science, Ewha Womans University, Seoul 120-750, Korea

Supporting Information

ABSTRACT: A new class of redox-active free base and metalloporphyrins fused with the 1,3-dithiol-2-ylidene subunits present in tetrathiafulvalene, termed MTTFP (M = H_2, Cu, Ni, Zn), have been prepared and characterized. The strong electron-donating properties of MTTFP were probed by electrochemical measurement and demonstrated that oxidation potentials can be tuned by metalation of the free base form, H_2TTFP. X-ray crystal structures of H_2TTFP, ZnTTFP, and CuTTFP revealed that a severe saddle-shape distortion was observed with the dithiole rings bent out of the plane toward one another in the neutral form. In contrast, the structure of the two-electron oxidized species ($CuTTFP^{2+}$) is planar, corresponding to a change from a nonaromatic to aromatic structure upon oxidation. A relatively large two-photon absorption (TPA) cross-section value of H_2TTFP^{2+} (1200 GM) was obtained for the free base compound, a value that is much higher than those typically seen for porphyrins (<100 GM). Augmented TPA values for the metal complexes were also seen. The strong electron-donating ability of ZnTTFP was further enhanced by binding of Cl^- and Br^- as revealed by thermal electron-transfer between ZnTTFP and Li^+-encapsulated C_{60} ($Li^+@C_{60}$) in benzonitrile, which was "switched on" by the addition of either Cl^- or Br^- (as the tetrabutylammonium salts). The X-ray crystal structure of Cl^--bound ZnTTFP was determined and provided support for the strong binding between the Cl^- anion and the Zn^{2+} cation present in ZnTTFP.

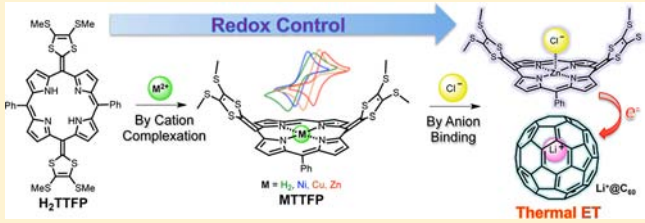

INTRODUCTION

Precise control and thorough understanding of the electronic structure and reactivity of redox-active molecules is of significant importance for the development of new catalysts and charge-separation devices, among other applications.[1−4] The exceptional optoelectronic and redox properties of porphyrins have driven efforts to prepare derivatives with more than one accessible and well-defined electronic state (e.g., aromatic, nonaromatic, and antiaromatic). In recent years, this challenge has been met in a number of instances via the use of so-called expanded porphyrins, analogues of porphyrins containing larger conjugated peripheries or a greater number of pyrrolic subunits than present in porphyrins.[5] However, there remains a need for smaller, electronically switchable materials that more closely resemble porphyrins. Of particular interest would be systems that provide for precise, tunable control of the redox potential over a range that allows for thermal electron transfer interactions with common donors or acceptors. Also of interest would be simple-to-prepare porphyrin analogues that allow access to stable $4n$ and $4n$ + 2 π-electron configurations, as well as intermediate $4n$ + 1 radical states.

Recently, we reported that a sterically restricted "rosarin", a hexapyrrolic expanded porphyrin, is capable of transitioning between its antiaromatic and reduced aromatic electronic forms via a stable one-electron oxidized radical state.[6] However, we are unaware of any tetrapyrrolic species that allow access to an analogous $4n$ + 1 π-electron radical oxidation state and that permit switching between two different closed-shell electronic

Received: May 18, 2013
Published: June 21, 2013

   dx.doi.org/10.1021/ja404830y | J. Am. Chem. Soc. 2013, 135, 10852−10862

states under standard laboratory conditions. Such putative tetrapyrrolic species are attractive since, in principle, their redox properties could be tuned by metalation as observed for normal porphyrins. Further fine-tuning of the redox properties could likewise be achieved by coordination of an axial ligand to a bound metal center.[7]

Here we report a new π-extended analogue of tetrathiafulvalene[8] (TTF), namely, the bis(1,3-dithiol-2-ylidene)quinoidal porphyrin (H_2TTFP) and its Cu(II), Ni(II), and Zn(II) derivatives (MTTFP; M = Cu^{II}, Ni^{II}, and Zn^{II}). In previous work, we reported TTF-bearing porphyrins wherein the TTF subunits were directly annulated to the porphyrin core.[9] MTTFP differs from these earlier systems in that it is a direct "extended" analogue of TTF. As such, it was expected to combine the desirable optical features of the known, but not extensively studied, quinoidal porphyrins[10] with the redox features of the so-called "exTTF" class of compounds [e.g., 9,10-bis(1,3-dithiol-2-ylidene)-9,10-dihydroanthracene].[11] As detailed below, this combination permits access to three stable oxidation states, as well as to the rich metalation chemistry of porphyrins. This latter attribute allows the electronic and redox properties of MTTFP to be tuned without additional synthetic modification. Additionally, complexation of either a chloride or bromide anion to a bound metal center permits fine-tuning of the redox properties of the MTTFP. This, in turn, enables control of electron transfer reactions, including specifically thermal processes involving transfer of an electron from ZnTTFP to Li^+-encapsulated C_{60} ($Li^+@C_{60}$) in benzonitrile (PhCN). This combination of chemical features, as well as the separate metal- and anion-based control of the redox properties, is not possible with the previously reported exTTF systems. Nor is it attainable with simple porphyrin derivatives. A further notable feature of the present system is that, in contrast to unmodified and dithiole-free quinoidal porphyrins, the MTTFPs reported herein display relatively large two-photon-absorption (TPA) cross-section values.

RESULTS AND DISCUSSION

Synthesis of MTTFP. The synthesis of H_2TTFP is shown in Scheme 1. It involves as the key step the triethyl phosphite-mediated cross-coupling between diketoporphyrinogen **2** and the known TTF precursor **3**.[33] The Lindsey group[12] has previously reported the preparation of **2**, through thallium-promoted oxidation of 5,15-diphenylporphine (**1**). However, in our hands, we found that compound **2** was more conveniently prepared (one step; 56% yield) by treating **1** with PbO_2 in accord with a decades-old procedure for the synthesis of xanthoporphryinogen.[13] Coupling of **2** and **3** then afforded the desired product H_2TTFP as an intensely colored dark green solid in 27% yield. The zinc(II) (ZnTTFP), copper(II) (CuTTFP), and nickel(II) (NiTTFP) complexes were then obtained in good yields by subjecting the free base to standard acetate salt metal insertion.[14]

A quinoidal structure, such as the one assigned to diketone **2**, was assigned to H_2TTFP and its metalated derivatives after examination of the ^{1}H NMR spectrum. Although *tautomerization* of the exocyclic double bonds would result in a fully conjugated core, H_2TTFP appears to be nonaromatic. This is consistent with what has been observed in the case of recently reported alkylidene porphyrins[10] and is specifically supported by the fact that the N−H protons within the porphyrinoid core resonate at 12.5 ppm (Figure 1; note that the full spectrum is shown in Figure S1 in the Supporting Information). In addition, the outer β-C−H protons of the pyrrolic rings give rise to signals at 6.5 and 6.9 ppm. Consequently, the ^{1}H NMR spectrum is strongly indicative of a lack of diatropic ring current and a corresponding lack of aromaticity in H_2TTFP. A nonaromatic quinoidal core is thus taken to be the dominant species in solution.

Scheme 1. Synthesis of H_2TTFP and Its Metal Derivatives, MTTFPs

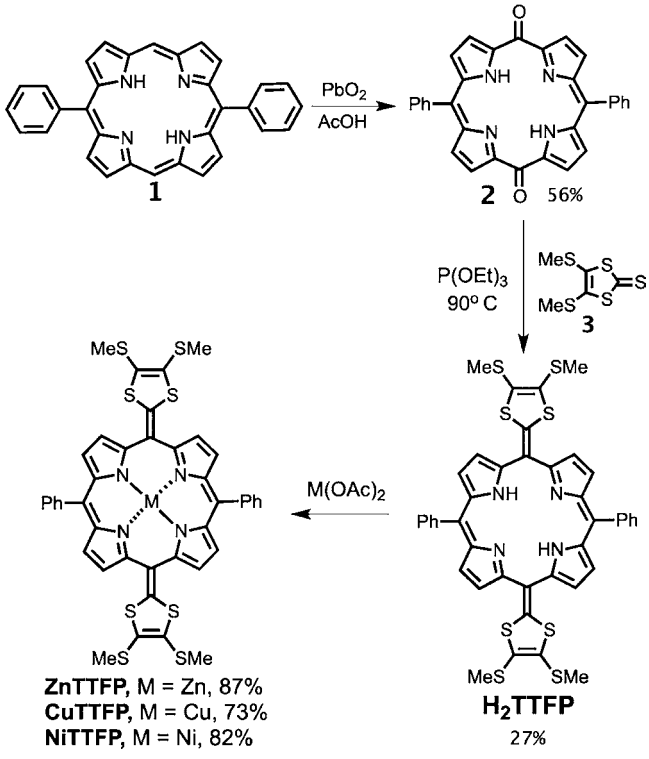

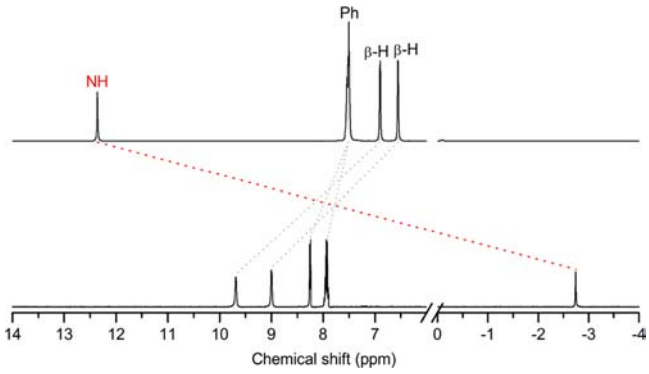

Figure 1. Partial ^{1}H NMR spectra of (top) H_2TTFP and (bottom) H_2TTFP·$2PF_6$, recorded in DMSO-d_6 at 298 K.

Spectroscopic Studies of MTTFP. In the case of MTTFP (M = Zn, Cu, Ni), evidence for metal complexation came from high-resolution mass spectrometric (HRMS) analyses. The ^{1}H NMR spectra of the diamagnetic Ni(II) and Zn(II) complexes revealed spectral patterns and chemical shifts similar to those for the corresponding β-pyrrolic and *meso*-phenyl proton signals of H_2TTFP (Figures S3 and S5, Supporting Information). A lack of N−H proton resonances is consistent with metal coordination within the macrocyclic core present in H_2TTFP. On the basis of these spectroscopic analyses, the resulting complexes, ZnTTFP and NiTTFP, were also assigned a quinoidal structure analogous to that of H_2TTFP.

dx.doi.org/10.1021/ja404830y | J. Am. Chem. Soc. 2013, 135, 10852−10862

An electron paramagnetic resonance (EPR) spectrum of CuTTFP recorded in CH_2Cl_2 at 298 K is typical of what is expected for a square planar Cu(II) complex with hyperfine interactions between the d^9-configured copper ion and the four magnetically equivalent ^{14}N atoms of the ligand (Figure 2a).

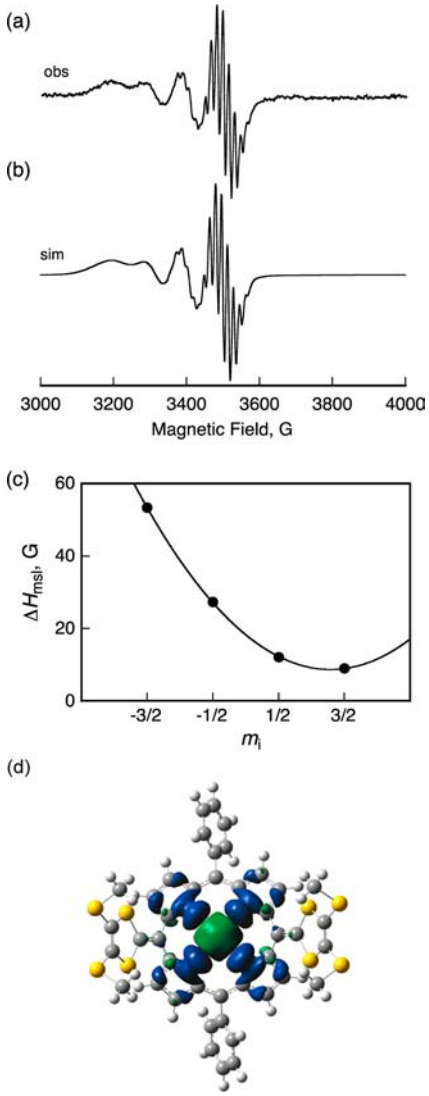

Figure 2. (a) EPR spectrum of CuTTFP recorded in CH_2Cl_2 at 298 K and (b) computer-simulated spectrum; a(Cu) = 91 G, a(4N) = 16 G, ΔH_{msl} = 53, 27, 12, and 9.0 G at $m_i = -3/2, -1/2, 1/2$, and $3/2$, respectively. (c) Plot of ΔH_{msl} vs m_i and (d) spin density map obtained from UB3LYP/LanL2DZ calculations.

The near-perfect agreement between the observed and simulated spectra was obtained with an isotropic g value of g = 2.090 and superhyperfine splitting of a(Cu) = 91 G and a(N) = 16 G by changing the line width (ΔH_{msl}) depending on the m_i values of Cu (Figure 2b,c). The observed a(Cu) value is smaller than those of typical Cu(II) porphyrin complexes.[15] This difference is ascribed to the fact that the unpaired electron density in CuTTFP is largely centered on the macrocycle and the associated orbital has $d_{x^2-y^2}$ character. This acts to delocalize ca. 50% of the spin density away from the copper center, as inferred from the theoretical spin density map obtained from UB3LYP/LanL2DZ calculations (Figure 2d).

The UV−visible spectrum of H_2TTFP recorded in CH_2Cl_2 at 298 K supports the assignment of the system as being nonaromatic. For instance, broad absorption bands are seen at λ_{max} = 650 nm (ε = 58 000 M^{-1}), 429 nm (ε = 53 700 M^{-1}), and 317 nm (ε = 38 700 M^{-1}) (Figure 3). These spectral

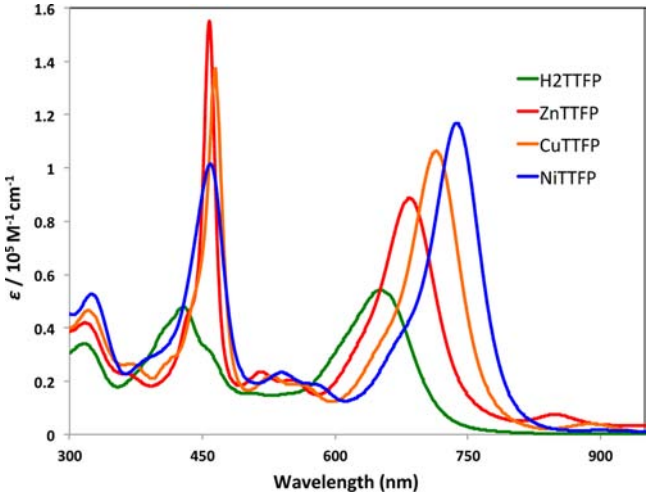

Figure 3. UV/vis absorption profiles of the metal derivatives of H_2TTFP recorded in CH_2Cl_2, including ZnTTFP (red), CuTTFP (orange), and NiTTFP (blue).

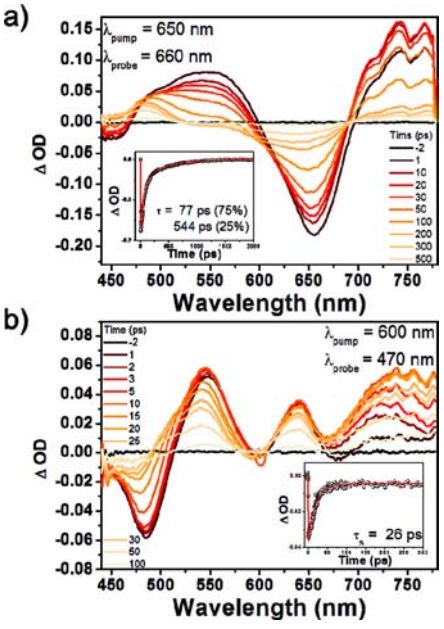

Figure 4. Femtosecond transient absorption spectra and time profiles of (a) free base H_2TTFP, recorded in toluene at 298 K, and (b) H_2TTFP·2ClO$_4$, recorded in acetonitrile at 298 K, obtained following excitation at 650 and 600 nm, respectively.

features resemble those of the reported quinoidal porphyrins.[16] The molecular orbitals (MOs), obtained from B3LYP/6-31G(d) calculations, provide support for the conclusion that the highest occupied molecular orbital (HOMO) is mainly localized on the dithiole subunits. In contrast, the lowest unoccupied molecular orbital (LUMO) is primarily centered within the macrocycle. This is taken as evidence that the

dx.doi.org/10.1021/ja404830y | J. Am. Chem. Soc. 2013, 135, 10852−10862

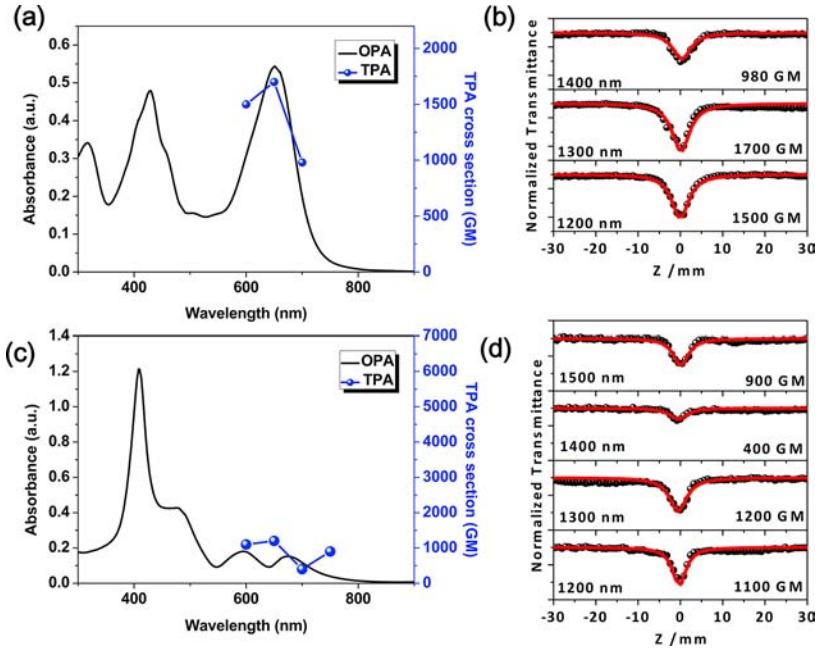

Figure 5. One-photon absorption (OPA) and two-photon absorption (TPA) spectra of (a) H_2TTFP and (c) H_2TTFP·2ClO_4 with (b, d) *Z*-scan curves recorded in CH_2Cl_2 and acetonitrile, respectively, at 298 K.

observed optical transition includes a contribution involving an intramolecular charge transfer from the dithiole subunits to the central macrocyclic core (cf. Figure S7, Supporting Information).[17] Upon metalation, similar low-energy broad absorption bands are seen (Figure 3) above 650 nm. The red shifts in these energy transitions follow the order ZnTTFP < CuTTFP < NiTTFP. In the case of ZnTTFP, a small intense band around 850 nm is typically seen in the UV−vis spectrum. This band is thought to reflect the presence of a radical cation impurity formed in small amounts under ambient aerobic conditions. The redox properties and dedicated formation of this and other oxidized forms of MTTFP are discussed later in the text.

The excited-state dynamics of H_2TTFP were further explored by femtosecond transient absorption (TA) spectroscopy in toluene. The transient species produced from H_2TTFP by femtosecond laser irradiation at 650 nm exhibited both broad excited-state absorption (ESA) and ground-state bleaching (GSB) features across the entire spectral region as shown in Figure 4a. The temporal profile of the prominent GSB signal at 660 nm was fitted to a biexponential function. This fitting revealed a short time constant of ≈77 ps, as well as a longer time constant (>500 ps) ascribed to a subsequent transition to the triplet manifold. Presumably, this latter intersystem crossing reflects the heavy atom effect of the sulfur atoms.

The TPA spectrum of H_2TTFP was also recorded in CH_2Cl_2 by the open aperture *Z*-scan method (Figure 5a,b). This analysis revealed spectral features coincident with the lowest one-photon absorption band. The maximum TPA cross-section value, $\sigma^{(2)}$ = 1700 GM, was attained upon excitation at 1300 nm. This value is notably larger than those for analogous (but dithiole-free) quinoidal porphyrins ($\sigma^{(2)}$ = ca. 500 GM at 1200 nm).[16] We propose that the unusual π-donor−π-acceptor−π-donor structure of H_2TTFP gives rise to the relatively enhanced nonlinear optical response. The TPA properties of the metal complexes MTTFPs (M = Zn, Ni, Cu) were also examined (Figure S9, Supporting Information). The ZnTTFP ($\sigma^{(2)}$ = 1100 GM at 1300 nm), NiTTFP ($\sigma^{(2)}$ = 510 GM at 1300 nm), and CuTTFP ($\sigma^{(2)}$ = 450 GM at 1300 nm) complexes gave values that were reduced compared to H_2TTFP but still relatively large with respect to the corresponding metalated porphryins.[18]

Crystal Structures and Redox Properties of MTTFP. Single crystals suitable for X-ray diffraction analysis of H_2TTFP (1:1 mixture of CH_2Cl_2 and acetonitrile), CuTTFP (CH_2Cl_2), and ZnTTFP (1:1 mixture of CH_2Cl_2 and tetrahydrofuran) were grown by slow evaporation. In all cases, a severe saddle-shape distortion was seen with the dithiole rings bent out of the plane toward one another (cf. Figure 6a,b and Figure S10, Supporting Information). A distinct lack of planarity is evident.

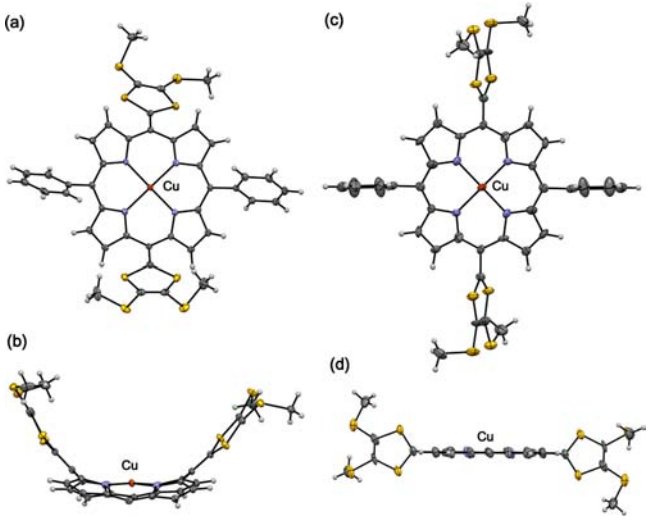

Figure 6. Crystal structures of CuTTFP (a, front view; b, side view) and of CuTTFP·2OTf (c, front view; d, side view). Thermal ellipsoids represent 50% probability. Triflate counteranions of CuTTFP·2OTf and *meso*-phenyl groups (in the side views) are omitted for clarity.

dx.doi.org/10.1021/ja404830y | J. Am. Chem. Soc. 2013, 135, 10852−10862

Such a finding provides support for the conclusion drawn from the spectroscopic analyses, namely, that the MTTFPs are nonaromatic.

The electrochemical properties of H_2TTFP and its metalated counterparts were further analyzed by cyclic voltammetry (CV) (Figure 7). In the case of the free base, H_2TTFP, a redox wave

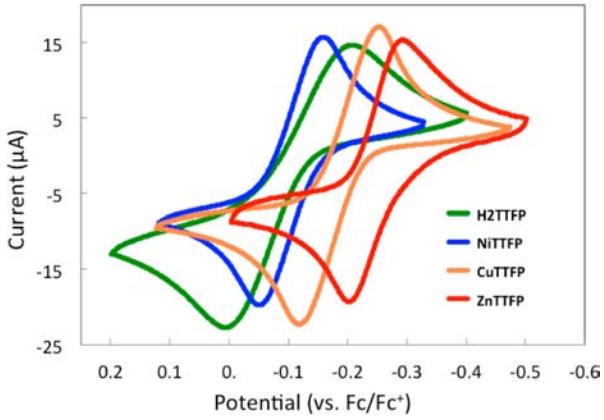

Figure 7. (a) Cyclic voltammograms (CVs) of H_2TTFP, NiTTFP, CuTTFP, and ZnTTFP [$E_{1/2}$ = −0.097, −0.105, −0.186, and −0.245 vs ferrocene/ferrocenium couple (Fc/Fc$^+$), respectively]. All CVs were recorded in CH_2Cl_2 at 298 K under identical conditions: 50 mV/s scan rate, 1 mM solution of the compound under study, 100 mM $TBAPF_6$.

at −0.10 V (vs ferrocene/ferrocenium couple, Fc/Fc$^+$) was seen. A cathodic/anodic peak separation of 215 mV was also seen in the case of the metal-free system. This was taken as initial evidence that a large conformational change occurs during this redox process. Shifts in the oxidation potentials were seen upon metalation. The nickel complex, NiTTFP, displayed a nominal shift of −0.008 V, making it only slightly easier to oxidize than the parent compound, H_2TTFP. However, complexes CuTTFP and ZnTTFP displayed marked anodic shifts to −0.186 and −0.245 V, respectively. These findings provide support for the notion that the oxidation potential of the bis(dithiole)quinoidal porphyrin H_2TTFP can be tuned by simple metal cation complexation.

Insight into the number of electrons being transferred during the oxidation of H_2TTFP and its metalated counterparts was inferred from the full CV of CuTTFP recorded in CH_2Cl_2 (Figure 8 and Figure S14, Supporting Information). A reversible one-electron feature ascribed to the reduction of CuTTFP is observed at −1.580 V, whose size is approximately half that of the TTFP oxidation peaks; on this basis, we propose that twice as many electrons are being transferred (2 e$^-$) in the TTFP oxidation as in the Cu reduction (1 e$^-$).[19]

Chemical Oxidation of H_2TTFP. The doubly oxidized form of H_2TTFP could also be prepared by chemical means (Scheme 2). Specifically, it was found that, by dissolving H_2TTFP in CH_2Cl_2 and adding an excess of crystalline nitrosyl hexafluorophosphate, the oxidized product could be precipitated from solution in quantitative yield in the form of its PF_6 salt (H_2TTFP·2PF_6). In a similar fashion, complexes with other counteranions were easily obtained by altering the identity of the oxidant used. The conversion of H_2TTFP to H_2TTFP^{2+} gave rise to distinctive spectral changes. In the ^{1}H NMR spectrum (Figure 1) of the dication, H_2TTFP·2PF_6, the N−H protons are shifted upfield to −2.8 ppm, while the β-hydrogens on the porphyrin core are shifted downfield. These changes are

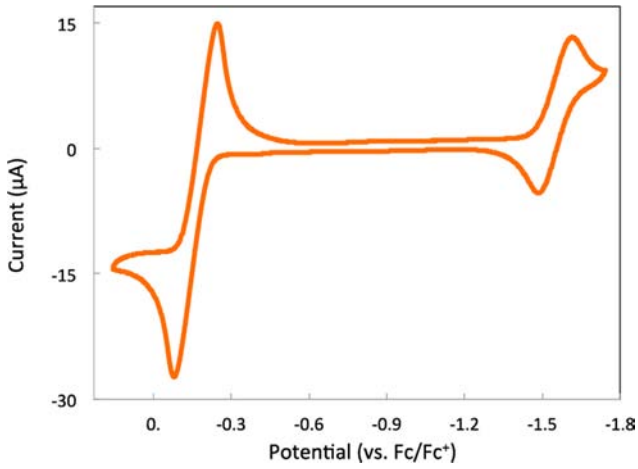

Figure 8. Cyclic voltammogram (CV) showing the first oxidation and reduction features of CuTTFP (referenced to Fc/Fc$^+$). The CV was recorded in CH_2Cl_2 at 298 K: 50 mV/s scan rate, 1 mM solution of the compound under study, 100 mM $TBAPF_6$.

thought to reflect the macrocyclic diamagnetic ring current of the central tetrapyrrolic unit. The negative NICS(0) values of −12.1 ppm at the center of the core macrocycle of H_2TTPF^{2+} provides further support for the assignment of H_2TTFP^{2+} as being aromatic (cf. Figure S13, Supporting Information).

A single-crystal X-ray diffraction structure of the doubly oxidized dication species derived from CuTTFP (i.e., CuTTFP·2OTf) revealed a highly planar geometry (Figure 6c,d and Figure S15, Supporting Information). The bond lengths between the dithiole rings and the *meso*-carbon atom of porphyrin also increased upon oxidation, as would be expected for the conversion of a C(sp^2)=C(sp^2) double bond (average length = 1.364 Å in the case of CuTTFP) to a single bond (length = 1.48 Å for CuTTFP·2OTf). These structural features are thus consistent with the proposed aromatic formulation.

The steady-state UV−vis absorption spectrum of H_2TTFP$_6$, recorded in acetonitrile at 298 K, revealed features characteristic of a porphyrin (e.g., tetraphenylporphyrin). For instance, well-resolved Q-like bands and an intense Soret band at 410 nm (ε = 121 000 M^{-1}) were seen (Figure 5b). The porphyrin-like MO density distribution of H_2TTFP^{2+} is in good agreement with the experimental spectrum (Figures S16 and S17, Supporting Information).[20] However, differences from normal porphyrins were revealed in the femtosecond TA spectra of the dication as recorded in acetonitrile. In particular, an ultrashort singlet excited-state lifetime of 26 ps (with a component with a prolonged decay profile ascribed to population of the triplet state) was seen in Figure 4b. This short lifetime[21] is consistent with the nonfluorescent nature of the dication and is thought to reflect electronic coupling with the dithiole moieties.

Further underscoring the differences relative to porphyrins (taken as ostensibly analogous control aromatic systems) is the relatively large TPA cross-section value of H_2TTFP^{2+}. Specifically, a TPA value of 1200 GM was recorded upon excitation at 1300 nm (Figure 5c,d). These values are considerably higher than those typically seen for porphyrins, for which TPA values of <100 GM are found.[18] These differences are ascribed to the charged dithiole sites that serve to perturb the intrinsic electronic structure of the central porphyrin core present in H_2TTFP^{2+}.[22]

The singly oxidized radical cation form, H_2TTFP$^{\bullet +}$, could be prepared in situ by the careful addition of tris(4-bromophenyl)-

dx.doi.org/10.1021/ja404830y | J. Am. Chem. Soc. 2013, 135, 10852−10862

Scheme 2. Stepwise Oxidation of H_2TTFP

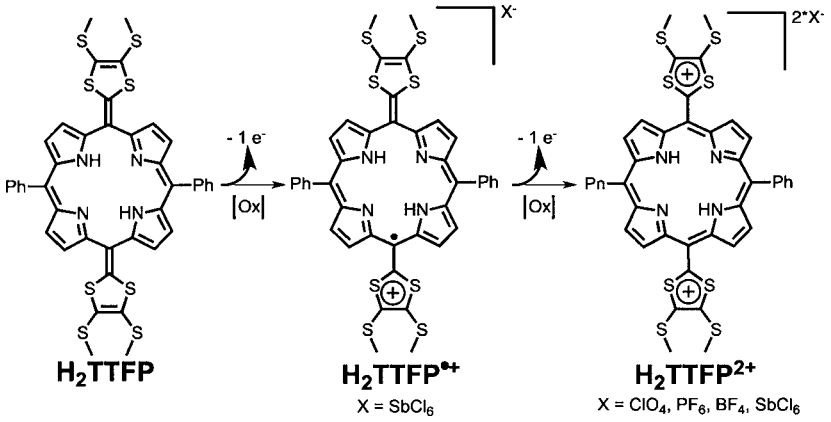

aminium hexachloroantimonate (so-called "magic blue") in CH_2Cl_2.[23] The formation of a species with an intense absorption band at 930 nm was seen, with a maximal intensity being observed upon the addition of 1 equiv of oxidant (Figure 9).[24] When less than one molar equivalent of magic blue is

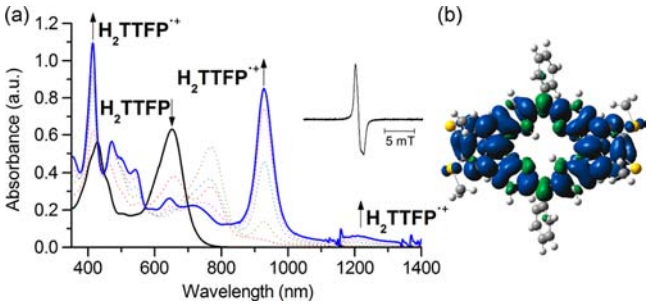

Figure 9. (a) UV/vis/near-IR absorption spectra of H_2TTFP recorded in CH_2Cl_2 at 298 K in the presence of increasing quantities of magic blue up to one molar equivalent; [H_2TTFP] = 10 μM. (Inset) EPR spectrum of $H_2TTFP^{\bullet+}$ (as the $SbCl_6^-$ salt) prepared via the addition of 1 equiv of magic blue. (b) Spin density map of $H_2TTFP^{\bullet+}$ obtained at the UB3LYP/6-31G(d) level.

added, a species with an absorption maximum (λ_{max}) at 760 nm is observed. This peak is thought to reflect protonation of H_2TTFP (for which enhanced acidity is expected due to the saddle-type distortion of the porphyrinoid core[24]) by residual acid present in the oxidant.[25] Support for this suggestion comes from the observation that adding trifluoroacetic acid to the free base species H_2TTFP in the absence of magic blue likewise gives rise to an analogous 760 nm spectral feature while leading to a decrease of the original absorption peak at 650 nm (Figure S18, Supporting Information). Furthermore, chemical oxidation of ZnTTFP (which lacks the basic pyrrolic sites present in H_2TTFP) with magic blue fails to produce a species with a $\lambda_{max} \approx 760$ nm (Figure S19, Supporting Information).

Electron paramagnetic resonance (EPR) spectroscopic analysis of $H_2TTFP^{\bullet+}$ (930 nm absorption band) revealed features at $g_\perp = 2.001$ and $g_\parallel = 2.006$ at 77 K,[26] thus supporting assignment of this oxidized species to the radical cation. Such readily accessible $4n + 1$ π-electron radical cation species are not attainable with either simple quinoidal porphyrins or the anthracene-derived exTTF species reported earlier. The behavior of MTTFP also stands in contrast to what is seen for the previously reported TTF porphyrins, where TTF-centered, but not porphyrinoid $4n+1$ π-electron, radicals may be observed[9]

The stability of $H_2TTFP^{\bullet+}$ proved to be highly dependent on the choice of solvent. In contrast to what was seen in pure CH_2Cl_2, in polar solvents, such as acetonitrile, PhCN, or mixtures of these solvents in CH_2Cl_2, the spectral features corresponding to $H_2TTFP^{\bullet+}$ were not observed (Figure S20, Supporting Information). This is ascribed to disproportionation of the radical cation $H_2TTFP^{+\bullet}$. Disproportionation leads to formation of the closed-shell neutral and dication forms of H_2TTFP, respectively, in analogy to what was found in the exTTFs.[27] An alternative explanation, involving dimerization to form a closed-shell, EPR-silent dimer (e.g., $[(H_2TTFP)_2]^{2+}$), is ruled out on steric grounds; the large *meso*-phenyl groups are expected to preclude the necessary intermolecular contact.

Fine Redox Control of ZnTTFP by Anion Binding. The strong electron-donor ability of ZnTTFP is further enhanced by axial coordination of chloride anion, Cl^-, as shown via its use as an external donor in a thermal electron transfer reaction. In these experiments, Li^+-encapsulated C_{60} ($Li^+@C_{60}$) was chosen as the electron acceptor, because $Li^+@C_{60}$ has a one-electron reduction potential [i.e., 0.13 V (vs standard calomel electrode, SCE)], which is slightly less positive than that of ZnTTFP (cf. Figure 7).[28] No evidence of electron transfer from ZnTTFP to $Li^+@C_{60}$ was seen in PhCN at 298 K. Specifically, addition of tetra-*n*-butylammonium perchlorate ($TBAClO_4$, 1.0 mM) to a PhCN solution of ZnTTFP and $Li^+@C_{60}$ resulted in no change in the optical features (Figure S21, Supporting Information). However, addition of chloride anion as TBACl to a PhCN solution containing ZnTTFP and $Li^+@C_{60}$ resulted in thermal electron transfer from ZnTTFP to $Li^+@C_{60}$. This is evidenced by the generation of spectral features ascribable to $ZnTTFP^{\bullet+}$ (λ_{max} = 865 nm) and $Li^+@C_{60}^{\bullet-}$ (λ_{max} = 1035 nm) as seen in Figure 10a.[28] The 1:1 stoichiometry of electron transfer between ZnTTFP and $Li^+@C_{60}$ in the presence of TBACl was confirmed by a Job plot (Figure S22, Supporting Information). The formation of $ZnTTFP^{\bullet+}$ and $Li^+@C_{60}^{\bullet-}$ was further confirmed by EPR spectral analyses, which revealed a superposition of signals corresponding to both species (Figure S23, Supporting Information). The yield of the electron-transfer products increased with increasing concentration of $Li^+@C_{60}$. The electron-transfer equilibrium constant (K_{et}), determined from the titration shown in Figure 10b, is 0.53.

The negative shift in the (two-electron) oxidation potential (E_{ox}) of ZnTTFP induced by binding of Cl^- was confirmed by

dx.doi.org/10.1021/ja404830y | J. Am. Chem. Soc. 2013, 135, 10852−10862

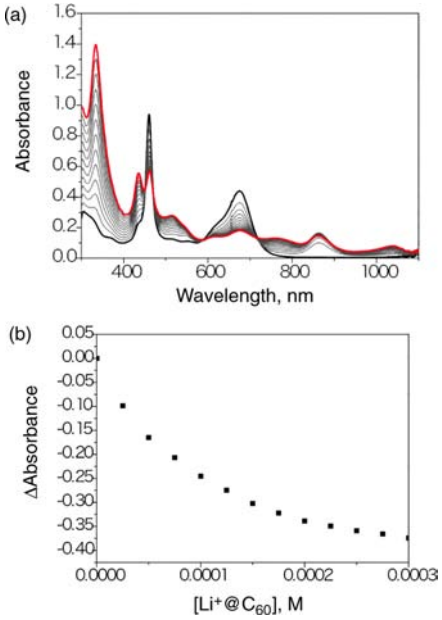

Figure 10. (a) UV/vis absorption changes in electron transfer from ZnTTFP (10 μM, black) to $Li^+@C_{60}$ (final, red) in the presence of 1.0 mM TBACl in PhCN at 298 K. (b) Plot of absorbance at 460 nm vs concentration of $Li^+@C_{60}$.

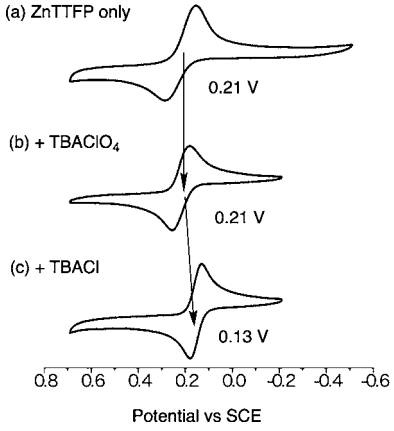

Figure 11. (a) Cyclic voltammogram (CV) of ZnTTFP (0.10 mM), recorded in the presence of $TBAPF_6$ (100 mM) in PhCN. (b) CV of ZnTTFP in the same solvent after the addition of $TBAClO_4$ (20 mM). (c) CV of ZnTTFP recorded under identical conditions after addition of TBACl (20 mM).

CV measurements, as shown in Figure 11. The E_{ox} value of ZnTTFP in the presence of $TBAPF_6$ in PhCN was determined to be 0.21 V versus SCE. The E_{ox} value remained the same after the addition of $TBAClO_4$. However, the addition of TBACl resulted in a cathodic shift of the E_{ox} value to 0.13 V versus SCE. Since the E_{red} value of $Li^+@C_{60}$ is 0.13 V versus SCE, electron transfer from ZnTTFP to $Li^+@C_{60}$ becomes thermodynamically feasible as the result of complexation of the Cl^- anion to ZnTTFP. The binding of Cl^- to ZnTTFP was confirmed via a single-crystal X-ray diffraction analysis. The resulting structure, shown in Figure 12, reveals that the Cl^- is coordinated to the Zn^{2+} center present in ZnTTFP.

The charge-separated species induced by the presence of chloride can be reverted to the neutral form via addition of excess pyridine; presumably this reflects competitive binding to the zinc center and displacement of the Cl^- ligand (Figure S24, Supporting Information). In this "molecular switch", the thermal electron transfer from ZnTTFP to $Li^+@C_{60}$ is "turned on" via addition of chloride and is "turned off" upon treatment with excess pyridine. This provides an additional level of control over a process that is not reflected in the chemistry of either exTTFs or quinoidal porphyrins.

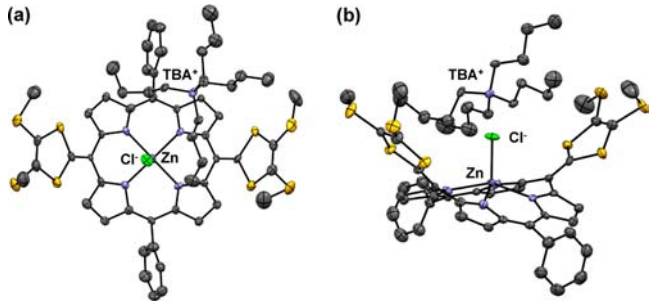

Figure 12. Two views of the single-crystal X-ray diffraction structure of ZnTTFP·TBACl at 50% thermal ellipsoid probability level. The solvent of crystallization and the hydrogen atoms are omitted for clarity.

$$\mathrm{ZnTTFP} + \mathrm{Li^+@C_{60}} \underset{\text{pyridine}}{\overset{\mathrm{Cl^-}}{\rightleftharpoons}} [\mathrm{Zn(Cl)TTFP}]^{\bullet} + [\mathrm{Li^+@C_{60}}]^{\bullet -}$$

As would be expected, complexation of Br^- to ZnTTFP also appears to be facile. This is evidenced by the fact that the addition of TBABr to a premixed PhCN solution of ZnTTFP and $Li^+@C_{60}$ also results in electron transfer from ZnTTFP to $Li^+@C_{60}$, in analogy to what is seen for Cl^- (Figure S25, Supporting Information).

CONCLUSION

In conclusion, we have synthesized a new class of quinoidal porphyrin analogues (MTTFPs) capable of existing in three distinct oxidation states, each separated by one electron. When subject to two-electron oxidation, aromatization is induced. This leads to conversion from a saddle-shaped nonaromatic species to a planar aromatic dicationic porphyrin, which exhibits a relatively large TPA cross-section value. The redox potentials of MTTFP may be tuned by metalation, with the associated electrochemical analyses revealing that MTTFP should be capable of acting as a strong electron donor. A particular advantage of these systems is that they are readily metalated and, as demonstrated by the zinc complex ZnTTFP, can ligate an axial ligand, thereby allowing the electronic properties to be tuned via two different modes (metal complexation and anion coordination). In the case where Cl^- or Br^- was bound to the zinc center of ZnTTFP, the electron-donor ability of the complex was further enhanced and this fine-tuning makes possible electron transfer from ZnTTFP to $Li^+@C_{60}$. Upon addition of pyridine to the chloride complex, back electron transfer took place, demonstrating the necessity of the Zn−halide bond for the forward reaction, as well as the versatility of the system.

The salient features of the MTTFPs—namely, access to three distinct $4n + y$ ($y = 0, 1, 2$) π-electron configurations, fine-tuning of the redox features through metal coordination and anion complexation, thermal electron transfer to $Li^+@C_{60}$, and high TPA values—are not observed in the case of either other easy-to-access tetrapyrrolic derivatives (including quinoidal porphyrins and TTF-porphyrins) or the anthracene-derived exTTF systems. We thus think that the present systems may

dx.doi.org/10.1021/ja404830y | J. Am. Chem. Soc. 2013, 135, 10852−10862

have a role to play in advancing our understanding of how modifications of relatively simple structures can be translated into potentially useful properties and electronic applications.

EXPERIMENTAL SECTION

Materials and General Methods. All chemicals were obtained from Acros Chemical Co. or TCI America in reagent-grade purity and used without further purification unless otherwise noted. PhCN was distilled over P_2O_5 immediately before use; the middle 50% was collected. Proton (400 MHz) and ^{13}C (100 MHz) NMR spectra were measured on a Varian 400/54/ASW instrument. Chemical shifts (δ scale) are reported in parts per million (ppm) relative to residual solvent and internal standard signals [deuterated dimethyl sulfoxide, DMSO-d_6 (2.50 ppm) and acetone-d_6 (2.05 ppm) for ^1H; CD_3Cl (77.2 ppm) and CD_3CN (1.3 ppm) for ^{13}C]. UV−visible−near-IR spectra were recorded on a Cary 5000 spectrometer in a 1 cm quartz cuvette. HRMS were recorded on an Agilent 6530 accurate mass quadrupole time-of-flight liquid chromatograph/mass spectrometer (QTOF/LC-MS) (with electrospray ionization, ESI) and a Ionospec 9.4 Fourier transform ion cyclotron resonance (FT-ICR) instrument (with matrix-assisted laser desorption ionization, MALDI).

Electrochemical Measurements. All electrochemical measurements were carried out on a CV-50 electrochemical analyzer in dichloromethane (CH_2Cl_2) at 298 K with 0.1 M $TBAPF_6$ as the supporting electrolyte. A glassy carbon working electrode was used, as well as a platinum wire counter electrode and an Ag/AgCl or Ag/$AgNO_3$ reference electrode. The working electrode was routinely polished by standard polishing procedures.

Electron Paramagnetic Resonance Measurements. The EPR spectra were recorded on a JEOL X-band spectrometer (JES-RE1XE) under nonsaturating microwave power conditions (1.0 mW) operating at 9.2 GHz. The magnitude of the modulation was chosen to optimize the resolution and the signal-to-noise ratio (S/N) of the observed spectrum (modulation width, 20 G; modulation frequency, 100 kHz). The g values were calibrated by use of an Mn^{2+} marker.

Femtosecond Transient Absorption Measurements. The femtosecond time-resolved transient absorption (TA) spectrometer consisted of a near-IR optical parametric amplifier system (Quantronix, Pallitra) pumped by a Ti:sapphire regenerative amplifier system (Quantronix, Integra-C) operating at 1 kHz repetition rate and an optical detection system. The generated output signals from the optical parametric amplifier had a pulse width of ∼100 fs in the range of 480−700 nm, which were used as pump pulses. White light continuum (WLC) probe pulses were generated by use of a sapphire window (3 mm thickness) by focusing a small portion of the fundamental 800 nm pulses. The time delay between pump and probe beams was carefully controlled by making the pump beam travel along a variable optical delay (Newport, ILS250). Intensities of the spectrally dispersed WLC probe pulses are monitored by two miniature spectrographs (OceanOptics USB2000+). To obtain the time-resolved transient absorption difference signal (ΔA) at a specific time, the pump pulses were chopped at 25 Hz and absorption spectra intensities were saved alternately with or without the pump pulse. Typically, 6000 pulses were used to excite the samples to obtain the TA spectra at a particular delay time. The polarization angle between pump and probe beam was set at the magic angle (54.7°) in order to prevent polarization-dependent signals. Cross-correlation full width at half-maximum (fwhm) in pump−probe experiments was less than 200 fs, and chirp of WLC probe pulses was measured to be 800 fs in the 400−1200 nm region. To minimize chirp, all reflection optics were used in the probe beam path and a 2 mm path length quartz cell was employed. After the TA experiments, the absorption spectra of all compounds were carefully checked so as to avoid artifacts arising from, e.g., photodegradation or photo-oxidation of the samples in question.

Two-Photon Absorption Experiments. Two-photon absorption (TPA) spectra were measured in the near-IR region by the open-aperture Z-scan method with 130 fs pulses from an optical parametric amplifier (Light Conversion, TOPAS) operating at a repetition rate of 2 kHz generated from a Ti:sapphire regenerative amplifier system (Spectra-Physics, Hurricane-X). The near-IR beam was divided into two parts. One was monitored by a Ge-PIN photodiode (New Focus) as an intensity reference, and the other was used for the transmittance measurement. After passing through a 10 cm focal length lens, the laser beam was focused and passed through a 1 mm quartz cell. Since the position of the sample cell could be controlled along the laser beam direction (z axis) by use of the motor-controlled delay stage, the local power density within the sample cell could be simply controlled under constant laser intensity. The transmitted laser beam from the sample cell was then detected by the same photodiode as used for reference monitoring. The on-axis peak intensity of the incident pulses at the focal point, I_0, ranged from 40 to 60 GW·cm^{-2}. For a Gaussian beam profile, the nonlinear absorption coefficient can be obtained by curve fitting of the observed open-aperture traces $T(z)$ with the following equation:

$$T(z) = 1 - \frac{\beta I_0 (1 - e^{-\alpha_0 l})}{2\sqrt{2}\,\alpha_0 [1 + (z/z_0)^2]}$$

where α_0 is the linear absorption coefficient, l is the sample length, and z_0 is the diffraction length of the incident beam. After the nonlinear absorption coefficient has been obtained, the TPA cross section $\sigma^{(2)}$ of one solute molecule (in units of GM, where 1 GM = 10^{-50} cm^4·s·photon^{-1}·molecule^{-1}) can be determined from the following relationship:

$$\beta = \frac{10^{-3}\sigma^{(2)} N_A d}{h\nu}$$

where N_A is the Avogadro constant, d is the concentration of the compound in solution, h is the Planck constant, and ν is the frequency of the incident laser beam.

Density Functional Theory Calculations. Theoretical calculations were performed with the Gaussian09 program suite on a supercomputer (KISTI, IBM).[29] All optimized structures were obtained via density functional theory (DFT) calculations with Becke's three-parameter hybrid exchange functionals and the Lee−Yang−Parr correlation functional (B3LYP) employing the 6-31G(d) basis set for all atoms.[30] The global ring centers for the NICS(0) (nucleus-independent chemical shift) values were designated at the nonweighted mean centers of the macrocycles. The NICS(0) value was obtained with gauge-independent atomic orbital (GIAO) method based on the optimized geometries. To simulate the ground-state absorption spectra, the time-dependent (TD) DFT calculation was employed with (U)B3LYP/6-31G(d) level. In the specific case of dication H2TTFP^{2+}, the long-range corrected TD-CAMB3LYP/6-31G(d) level calculations of Handy and co-workers[31] that give rise to consistent transitions for charged derivatives were carried out.

Synthetic Procedures. *5,15-Dioxo-10,20-diphenylporphodimethene (**2**).* 5,15-Diphenylporphyrin (**1**) (0.77 g, 1.66 mmol) was dissolved in a mixture of chloroform (100 mL) and acetic acid (20 mL). A solution of PbO_2 (4.0 g, 16.7 mmol) was added and the reaction mixture was stirred for 5 h open to air, whereafter the mixture was slowly poured into a saturated aqueous sodium bicarbonate solution (300 mL) to quench the acetic acid, and the organic and aqueous phase were separated. The organic phase was passed through a short plug of Celite to remove residual lead salts. The aqueous layer was extracted twice with dichloromethane (2 × 100 mL), and the two organic fractions were also passed through the Celite. The Celite was washed thoroughly with dichloromethane until the filtrate was colorless. The combined organic filtrates were evaporated and the residue was purified by column chromatography over silica gel with 30% hexanes/dichloromethane as the eluent. The dark yellow band was collected, affording 0.46 g (56% yield) of **2** as a black solid. The black crystalline solid could be further purified by recrystallization from hot toluene. The ^1H NMR spectral data matched those reported previously:[30] ($CDCl_3$, 298 K) δ 6.2−2.6 (br s, 4H, β-H), 7.17 (d, J = 4.4 Hz, 4H, β-H), 7.35−7.45 (m, 10H, Ph-H), 13.85 (br s, 2H, N−H) ppm.

ExTTF-Porphyrin (H_2TTFP). To a mixture of 5,15-dioxo-10,20-diphenylporphodimethene (**2**) 100 mg, 0.203 mmol) and 4,5-

dx.doi.org/10.1021/ja404830y | J. Am. Chem. Soc. 2013, 135, 10852−10862

bis(methylthio)-1,3-dithiole-2-thione (**3**)[33] (100 mg, 0.444 mmol) in a dried 100 mL round-bottom flask was added freshly distilled triethyl phosphite (3 mL), and the reaction mixture was heated slowly to 90 °C under a nitrogen atmosphere. After the reaction mixture was stirred for 1 h at 90 °C, another 100 mg (0.444 mmol) aliquot of **3** was added. The mixture was stirred for an additional 1 h, affording a dark green solution. After cooling to room temperature, the reaction mixture was filtered through a fine-fritted glass filter to give a dark green solid as a "first crop". The remaining filtrate was poured into cold methanol (100 mL) and the resulting precipitate was collected by filtration to yield a "second crop". The first crop obtained in this way proved sufficiently pure to be used in further reactions. The second crop was purified by column chromatography over silica gel (to remove the product of the homocoupling of **3**) with 30% hexanes/dichloromethane as the eluent; this provided analytically pure H_2TTFP (total yield, 102 mg, 27%). R_f = 0.3; ^{1}H NMR (acetone-d_6, 298 K) δ 2.48 (s, 12H, S-CH_3), 6.61 (d, J = 4.3 Hz, 4H, β-H), 6.90 (d, J = 4.3 Hz, 4H, β-H), 7.55 (m, 10H Ph-H) 12.59 (s, 2H, NH); ^{13}C NMR ($CDCl_3$, 298 K) δ 19.1, 114.1, 117.9, 127.4, 127.9, 128.5, 129.6, 130.9, 138.0, 140.0, 141.7, 152.3; HRMS (positive ESI) m/z 849.04578, calcd 849.04654; MP > 300 °C.

Oxidation of H_2TTFP to H_2TTFP·2PF_6. Free base H_2TTFP (20 mg, 0.024 mmol) was dissolved in a minimal amount of dichloromethane (2 mL). Crystalline $NOPF_6$ (≈ 45 mg, 0.257 mmol) was quickly weighed and added in excess, and the reaction was stirred for 15 min. A precipitate was immediately noticeable. After 15 min, the residual solvent proved to be nearly colorless, and at this time the solvent and precipitate were decanted from the leftover solid $NOPF_6$. The solution was filtered and the solids were washed with water and dichloromethane until the filtrate was colorless. The solid material was dried under vacuum at room temperature to give pure H_2TTFP·2PF_6. ^{1}H NMR (DMSO-d_6, 298 K) δ −2.75 (s, 2H, NH), 3.11 (s, 12H, S-CH_3), 7.92 (m, 6H, Ph-H), 8.24 (dd, J = 1.45, 7.75), 8.99 (br s, 4H, β-H), 9.68 (br s, 4H, β-H); ^{13}C NMR ($CDCl_3$, 125 MHz, 298 K) δ 19.4, 125.9, 127.0, 128.4, 131.3, 134.3, 134.5, 141.4, 148.9, 152.0, 155.5; HRMS (positive ESI) for z = 1, m/z 849.046 93, calcd 849.046 54; for z = 2, m/z 425.027 27, calcd 425.02691; mp > 300 °C.

General Metalation Procedure for H_2TTFP. Compound H_2TTFP (20 mg, 0.024 mmol) was dissolved in dichloromethane (50 mL) and excess metal acetate $M(OAc)_2$ (100 mg) dissolved in MeOH (1 mL) was added. The solution was stirred for 1 h or until all H_2TTFP was consumed, as judged by thin-layer chromatography (TLC) analysis. After removal of the solvent, the residue was purified by column chromatography over silica gel to give the target complexes,:

ZnTTFP. Eluent dichloromethane; R_f = 0.8 (87% yield); ^{1}H NMR (DMSO-d_6, 400 MHz, 298 K) δ 2.43 (s, 12H, S-CH_3), 6.40 (d, J = 4.2 Hz, 4H, β-H), 6.85 (d, J = 4.2 Hz, 4H, β-H), 7.47 (m, Ph-H); ^{13}C NMR ($CDCl_3$, 125 MHz, 298 K) δ 19.0 116.3, 117.8, 127.1, 127.5, 128.0, 130.7, 131.6, 139.5, 141.7, 155.7; HRMS (positive MALDI) m/z 909.9524, calcd 909.9522; mp > 300 °C. This compound was further analyzed by single-crystal X-ray diffraction analysis.

CuTTFP. Eluent 30% hexanes/dichloromethane; R_f = 0.9 (73% yield). As noted under Spectroscopic Studies of MTTFP, the EPR spectrum of this complex is consistent with the proposed structure. A clean HPLC chromatogram of this paramagnetic species was also obtained. HRMS (positive MALDI) m/z 908.9516, calcd 908.9527; mp > 300 °C. This compound was further analyzed by single-crystal X-ray diffraction analysis.

NiTTFP. Eluent dichloromethane; R_f = 0.9 (82% yield). ^{1}H NMR (DMSO-d_6, 400 MHz, 298 K) δ 2.46 (s, 12H, S-CH_3), 6.65 (d, J = 4.5 Hz, 4H, β-H), 6.89 (d, J = 4.5 Hz, 4H, β-H), 7.52 (m, 10H, Ph-H). ^{13}C NMR could not be taken due to precipitation from DMSO-d_6 upon standing over several hours. HRMS (positive MALDI) m/z 903.9587, calcd 903.9584; mp > 300 °C.

Preparation of ZnTTFP·TBACl. For absorption and CV studies, ZnTTFP·TBACl was prepared in situ by the addition of 1.2 mol equiv of tetrabutylammonium chloride to ZnTTFP in PhCN. ZnTTFP·TBACl can be isolated as its crystalline salt by the addition of 3 mol equiv of tetrabutylammonium chloride to ZnTTFP in dichloromethane followed by slow diffusion of hexanes at 277 K for several days.

X-ray Crystallography Methods. All data were collected on a Rigaku ACF-12 with a Saturn 724+ CCD and a Rigaku SCX-Mini diffractometer with a Mercury 2 charge-coupled device (CCD) by use of a graphite monochromator with Mo Ka radiation (λ = 0.710 75 Å). The data were collected at 100 K on a Rigaku XStream low-temperature device. Details of crystal data, data collection, and structure refinement for each analyzed sample are listed in Supporting Information. In all cases, data reduction was performed with Rigaku Americas Corporation's Crystal Clear version 1.40.[34] Each structure was solved by direct methods using SIR97[35] and refined by full-matrix least-squares on F^2 with anisotropic displacement parameters for the non-H atoms using SHELXL-97.[36] Contributions to the scattering factors due to the solvent molecules were removed by use of the utility SQUEEZE[37] in PLATON98.[38] Structure analysis was aided by use of PLATON98 as incorporated into WinGX.[39] The hydrogen atoms on carbon were calculated in ideal positions with isotropic displacement parameters set to 1.2xUeq of the attached atom (1.5xUeq for methyl hydrogen atoms). Definitions used for calculating $R(F)$, $R_w(F^2)$, and goodness of fit, S, are given in Supporting Information.[40] The data were checked for secondary extinction effects but no correction was necessary. Neutral atom scattering factors and values used to calculate the linear absorption coefficient are from the International Tables for X-ray Crystallography (1992).[41] All figures were generated with SHELXTL/PC.[42] Details of the structures and their refinement may be obtained from the Cambridge Crystallographic Data Centre by referencing CCDC 931728 for H_2TTFP, 931726 for CuTTFP, 931727 for CuTTFP·2OTf, 931725 for ZnTTFP, and 0001834 for ZnTTFP·TBACl.

■ ASSOCIATED CONTENT

Supporting Information

Additional text, 26 figures, and 31 tables with characterization data for all new compounds and X-ray crystallographic data (pdf); crystallographic files (cif). This material is available free of charge via the Internet at http://pubs.acs.org.

■ AUTHOR INFORMATION

Corresponding Author

sessler@cm.utexas.edu; dongho@yonsei.ac.kr; fukuzumi@chem.eng.osaka-u.ac.jp

Notes

The authors declare no competing financial interest.

■ ACKNOWLEDGMENTS

Support is acknowledged from the U.S. National Science Foundation (CHE-1057904 to J.L.S.), the Robert A. Welch Foundation (F-1018 to J.L.S.), JSPS (20108010 to S.F.), the World Class University (WCU) program (R32-2012-000-10217-0 to D.K, R31-2008-000-10010-0 to S.F.) of the Ministry of Education, Science and Technology, the Villum Foundation (to J.O.J.), and The Danish Natural Science Reasearch Council (FNU, Project 11-106744 to J.O.J.).

■ REFERENCES

(1) (a) Frischmann, P. D.; Mahata, K.; Würthner, F. *Chem. Soc. Rev.* **2013**, *42*, 1847−1870. (b) Li, L.-L.; Diau, E. W.-G. *Chem. Soc. Rev.* **2013**, *42*, 291−304. (c) Bottari, G.; Trukhina, O.; Ince, M.; Torres, T. *Coord. Chem. Rev.* **2012**, *256*, 2453−2477. (d) Griffith, M. J.; Sunahara, K.; Wagner, P.; Wagner, K.; Wallace, G. G.; Officer, D. L.; Furube, A.; Katoh, R.; Mori, S.; Mozer, A. J. *Chem. Commun.* **2012**, *48*, 4145−4162. (e) Panda, M. K.; Ladomenou, K.; Coutsolelos, A. G. *Coord. Chem. Rev.* **2012**, *256*, 2601−2627.

(2) (a) Wasielewski, M. R. *Acc. Chem. Res.* **2009**, *42*, 1910−1921. (b) Wasielewski, M. R. *J. Org. Chem.* **2006**, *71*, 5051−5066.

(3) (a) Malig, J.; Jux, N.; Guldi, D. M. *Acc. Chem. Res.* **2013**, *46*, 53−64. (b) Goerl, D.; Zhang, X.; Wuerthner, F. *Angew. Chem., Int. Ed.* **2012**, *51*, 6328−6348.
(4) (a) Fukuzumi, S.; Yamada, Y.; Suenobu, T.; Ohkubo, K.; Kotani, H. *Energy Environ. Sci.* **2011**, *4*, 2754−2766. (b) Fukuzumi, S.; Ohkubo, K. *J. Mater. Chem.* **2012**, *22*, 4575−4587. (c) Fukuzumi, S.; Honda, T.; Kojima, T. *Coord. Chem. Rev.* **2012**, *256*, 2488−2502.
(5) (a) Saito, S.; Osuka, A. *Angew. Chem., Int. Ed.* **2011**, *50*, 4342−4373. (b) Osuka, A.; Saito, S. *Chem. Commun.* **2011**, *47*, 4330−4339. (c) Roznyatovskiy, V. V.; Lee, C.-H.; Sessler, J. L. *Chem. Soc. Rev.* **2013**, *42*, 1921−1933.
(6) Ishida, M.; Kim, S.-J.; Preihs, C.; Ohkubo, K.; Lim, J. M.; Lee, B. S.; Park, J. S.; Lynch, V. M.; Roznyatovskiy, V. V.; Sarma, T.; Panda, P. K.; Lee, C.-H.; Fukuzumi, S.; Kim, D.; Sessler, J. L. *Nat. Chem.* **2013**, *5*, 15−20.
(7) (a) *The Porphyrin Handbook, Volume 3, Inorganic, Organometallic, and Coordination Chemistry*; Kadish, K. M., Smith, K. M., Guilard, R., Eds.; Academic Press: San Diego, CA, 2000. (b) Park, J. S.; Karnas, E.; Ohkubo, K.; Chen, P.; Kadish, K. M.; Fukuzumi, S.; Bielawski, C.; Hudnall, T. W.; Sessler, J. L. *Science* **2010**, *329*, 1324−1327. (c) Fukuzumi, S.; Ohkubo, K.; D'Souza, F.; Sessler, J. L. *Chem. Commun.* **2012**, *48*, 9801−9815.
(8) (a) Schukat, G.; Fanghänel, E. *Sulfur Rep.* **1996**, *18*, 1−294. (b) Bryce, M. R. *J. Mater. Chem.* **2000**, *10*, 589−598. (c) Segura, J. L.; Martín, N. *Angew. Chem., Int. Ed.* **2001**, *40*, 1372−1409. (d) Jeppesen, J. O.; Nielsen, M. B.; Becher, J. *Chem. Rev.* **2004**, *104*, 5115−5132. (e) Inagi, S.; Naka, K.; Chujo, Y. *J. Mater. Chem.* **2007**, *17*, 4122−4135. (f) Martín, N.; Sánchez, L.; Herranz, M. a. Á.; Illescas, B.; Guldi, D. M. *Acc. Chem. Res.* **2007**, *40*, 1015−1024. (g) Lorcy, D.; Bellec, N.; Fourmigué, M.; Avarvari, N. *Coord. Chem. Rev.* **2009**, *253*, 1398−1438.
(9) (a) Becher, J.; Brimert, T.; Jeppesen, J. O.; Pedersen, J. Z.; Zubarev, R.; Bjørnholm, T.; Reitzel, N.; Jensen, T. R.; Kjaer, K.; Levillain, E. *Angew. Chem., Int. Ed.* **2001**, *40*, 2497−2500. (b) Li, H.; Jeppesen, J. O.; Levillain, E.; Becher, J. *Chem. Commun.* **2003**, 846−847. (c) Nielsen, K. A.; Levillain, E.; Lynch, V. M.; Sessler, J. L.; Jeppesen, J. O. *Chem.—Eur. J.* **2009**, *15*, 506−516. (d) Jana, A.; Ishida, M.; Kwak, K.; Sung, Y. M.; Kim, D.-S.; Lynch, V. M.; Lee, D.; Kim, D.; Sessler, J. L. *Chem.—Eur. J.* **2013**, *19*, 338−349.
(10) Lee, C.-H.; Roznyatovskiy, V. V.; Hong, S.-L.; Sessler, J. L. in *Handbook of Porphyrin Science*; Kadish, K. M., Smith, K. M., Guilard, R., Eds.; World Scientific, Singapore, 2011; pp 197−252.
(11) (a) *TTF Chemistry*; Yamada, J., Sugimoto, T., Eds.; Kodansha Ltd.: Tokyo, 2004. (b) Brunetti, F. G.; Lopez, J. L.; Atienza, C.; Martin, N. *J. Mater. Chem.* **2012**, *22*, 4188−4205.
(12) Lahaye, D.; Muthukumaran, K.; Hung, C.-H.; Gryko, D.; Reboucas, J. S.; Spasojevic, I.; Batinic-Haberle, I.; Lindsey, J. S. *Bioorg. Med. Chem.* **2007**, *15*, 7066−6086.
(13) (a) Fischer, H.; Treibs, A. *Annalen* **1927**, *457*, 209−248. (b) Inhoffen, H. H.; Fuhrhop, J. R.; von der Haar, F. *Justus Liebigs Ann. Chem.* **1966**, *700*, 92−105.
(14) *The Porphyrin Handbook, Volume 1, Synthesis and Organic Chemistry*; Kadish, K. M., Smith, K. M., Guilard, M. R., Eds.; Academic Press: San Diego, CA, 2000.
(15) Cunningham, K. L.; McNett, K. M.; Pierce, R. A.; Davis, K. A.; Harris, H. H.; Falck, D. M.; McMillin, D. R. *Inorg. Chem.* **1997**, *36*, 608−613.
(16) Zeng, W.; Lee, B. S.; Sung, Y. M.; Huang, K.-W.; Li, Y.; Kim, D.; Wu, J. *Chem. Commun.* **2012**, *48*, 7684−7686.
(17) Similar conclusions were drawn in the case of simple exTTF derivatives: Diaz, M. C.; Illescas, B. M.; Martin, N.; Viruela, R.; Viruela, P. M.; Orti, E.; Brede, O.; Zilbermann, I.; Guldi, D. M. *Chem.−Eur. J.* **2004**, *10*, 2067−2077.
(18) TPA cross-section values for reference metalated tetraphenylporphyrins (MTPP) have been reported as follows: For ZnTPP, (a) Drobizhev, M.; Karotki, A.; Kruk, M.; Rebane, A. *Chem. Phys. Lett.* **2002**, *355*, 175−182. For NiTPP, (b) Yoon, M.-C.; Noh, S.-B.; Tsuda, A.; Nakamura, Y.; Osuka, A.; Kim, D. *J. Am. Chem. Soc.* **2007**, *129*, 10080−10081. For CuTPP, (c) Morone, M.; Beverina, L.; Abbotto, A.; Silvestri, F.; Collini, E.; Ferrante, C.; Bozio, R.; Pagani, G. A. *Org. Lett.* **2006**, *8*, 2719−2722.
(19) This conclusion is based on the assumption that the system is under diffusion control; it was confirmed by varying the scan rate and plotting the square root of the scan rate versus the intensity of the redox peak yielding a linear plot (cf. Figure S14, Supporting Information).
(20) Goutermann, M. in *The Porphyrins*; Dolphin, D., Ed.; Academic: New York, 1978.
(21) Typical metal-free porphyrin lifetimes are on the order of nanoseconds.
(22) The choice of the counteranion (OTf^-, BF_4^-, or ClO_4^-) does not appear to affect significantly the properties of dication $H2TTFP^{2+}$.
(23) The radical cation form of "exTTF" quickly disproportionates in the same solvent: Guldi, G. M.; Sanchez, L.; Martin, N. *J. Phys. Chem. B* **2001**, *105*, 7139−7144.
(24) (a) Shen, Y.; Ryde, U. *Chem.—Eur. J.* **2005**, *11*, 1549. (b) Bain-Ackerman, M. J.; Lavallee, D. K. *Inorg. Chem.* **1979**, *18*, 3358.
(25) Todres, Z. V. *Ion-Radical Organic Chemistry: Principles and Applications*, 2nd ed.; CRC Press: Boca Raton, FL, 2009.
(26) Calculations reveal that the spin density on the nitrogen atoms of $H_2TTFP^{\bullet+}$ is relatively delocalized. This is consistent with the absence of appreciable hyperfine coupling seen in the EPR spectrum.
(27) Frere, P.; Allain, M.; Elandaloussi, E. H.; Levillain, E.; Sauvage, F.-X.; Riou, A.; Roncali, J. *Chem.−Eur. J.* **2002**, *8*, 784−792.
(28) (a) Kawashima, Y.; Ohkubo, K.; Fukuzumi, S. *J. Phys. Chem. A* **2012**, *116*, 8942−8948. (b) Fukuzumi, S.; Ohkubo, K.; Kawashima, Y.; Kim, D. S.; Park, J. S.; Jana, A.; Lynch, V. M.; Kim, D.; Sessler, J. L. *J. Am. Chem. Soc.* **2011**, *133*, 15938−15941.
(29) Frisch, M. J.; Trucks, G. W.; Schlegel, H. B.; Scuseria, G. E.; Robb, M. A.; Cheeseman, J. R.; Scalmani, G.; Barone, V.; Mennucci, B.; Peterson, G. A.; Nakatsuji, H.; Caricato, M.; Li, X.; Hratchian, H. P.; Izmaylov, A. F.; Bloino, J.; Zheng, G.; Sonnenberg, J. L.; Hada, M.; Ehara, M.; Toyota, K.; Fukuda, R.; Hasegawa, J.; Ishida, M.; Nakajima, T.; Honda, Y.; Kitao, O.; Nakai, H.; Vreven, T.; Montgomery, J. A., Jr.; Peralta, J. E.; Ogliaro, F.; Bearpark, M.; Heyd, J. J.; Brothers, E.; Kudin, K. N.; Staroverov, V. N.; Kobayashi, R.; Normand, J.; Raghavachari, K.; Rendell, A.; Burant, J. C.; Iyengar, S. S.; Tomasi, J.; Cossi, M.; Rega, N.; Millam, N. J.; Klene, M.; Knox, J. E.; Cross, J. B.; Bakken, V.; Adamo, C.; Jaramillo, J.; Gomperts, R.; Stratmann, R. E.; Yazyev, O.; Austin, A. J.; Cammi, R.; Pomelli, C.; Ochterski, J. W.; Martin, R. L.; Morokuma, K.; Zakrzewski, V. G.; Voth, G. A.; Salvador, P.; Dannenberg, J. J.; Dapprich, S.; Daniels, A. D.; Farkas, Ö.; Foresman, J. B.; Ortiz, J. V.; Cioslowski, J.; Fox, D. J. *Gaussian 09, Revision A.1*; Gaussian Inc., Wallingford, CT, 2009.
(30) (a) Becke, A. D. *Phys. Rev. A* **1988**, *38*, 3098. (b) Lee, C.; Yang, W.; Parr, R. G. *Phys. Rev. B* **1988**, *37*, 785.
(31) Yanai, T.; Tew, D.; Handy, N. *Chem. Phys. Lett.* **2004**, *393*, 51−57.
(32) Lahaye, D.; Muthukumaran, K.; Hung, C.-H.; Gryko, D.; Reboucas, J. S.; Spasojevic, I.; Batinic-Haberle, I.; Lindsey, J. S. *Bioorg. Med. Chem.* **2007**, *15*, 7066−7086.
(33) Steimecke, G.; Sieler, H. J.; Kirmse, R.; Hoyer, E. *Phosphorus Sulfur* **1979**, *7*, 49−55. (b) Simonsen, K. B.; Svenstrup, N.; Lau, J.; Simonsen, O.; Mork, P.; Kristensen, G. J.; Becher, J. *Synthesis* **1996**, 407−418.
(34) *Crystal Clear 1.40*; Rigaku Americas Corp., The Woodlands, TX, 2008.
(35) Altomare, A.; Burla, M. C.; Camalli, M.; Cascarano, G. L.; Giacovazzo, C.; Guagliardi, A.; Moliterni, A. G. G.; Polidori, G.; Spagna, R. *J. Appl. Crystallogr.* **1999**, *32*, 115−119.
(36) Sheldrick, G. M. *Acta Crystallogr.* **2008**, *A64*, 112−122.
(37) Sluis, P. v. d.; Spek, A. L. *Acta Crystallogr.* **1990**, *A46*, 194−201.
(38) Spek, A. L *PLATON, A Multipurpose Crystallographic Tool*; Utrecht University, The Netherlands, 1998.
(39) Farrugia, L. J. *J. Appl. Crystallogr.* **1999**, *32*, 837−838.
(40) $R_w(F^2) = \{\sum_w(|F_o|^2 - |F_c|^2)^2/\sum_w(|F_o|)^4\}^{1/2}$, where w is the weight given each reflection. $R(F) = \Sigma(|F_o| - |F_c|)/\Sigma(|F_o|)$ for reflections with $F_o > 4[\sigma(F_o)]$. $S = [\Sigma_w((|F_o|^2 - |F_c|^2)^2/(n - p)]^{1/2}$,

where n is the number of reflections and p is the number of refined parameters.
(41) Tables 4.2.6.8 and 6.1.1.4. In *International Tables for X-ray Crystallography, Vol. C*; Wilson, A. J. C., Ed.; Kluwer Academic Press: Boston, 1992.
(42) Sheldrick, G. M. *SHELXTL/PC (version 5.03)*; Siemens Analytical X-ray Instruments, Inc., Madison, WI, 1994.